Investigation of the Firing Stability of a Combat Robot on an Elastic Foundation

Dang Ba Ngoc
PHD Student
Department of Weapons and Ammunition
University of Defence
Faculty of Military Technology
Czech Republic

Martin Macko
Professor
Department of Weapons and Ammunition
University of Defence
Faculty of Military Technology
Czech Republic

Jiří Balla
Professor
Department of Weapons and Ammunition
University of Defence
Faculty of Military Technology
Czech Republic

This paper investigates the vibration of a combat robot–weapon system equipped with a small-caliber automatic weapon during firing, based on a physical and mathematical model developed using multibody system dynamics theory. The spatial model of the combat robot features six degrees of freedom (DOF), encompassing a controlled robot equipped with a 5.56 mm automatic rifle. The weapon dynamics, represented by the displacement of the base link, are analyzed simultaneously with the vibrations of the entire system. By applying numerical methods to solve the system of differential equations describing the vibrations induced by firing forces, while taking into account the elastic properties of the supporting ground, the dynamic response of the robot–weapon system was investigated. Experimental measurements of the robot's vibrations in the firing plane demonstrated excellent agreement with the theoretical simulations, confirming the validity of the proposed model. The proposed model enables the identification of the key parameters affecting the firing stability of the robot. The calculated results exhibit a reasonable degree of reliability, providing a scientific foundation for further research on system stability and weapon accuracy when integrated into a combat robot.

***Keywords:** Vibration, Combat robot, Weapon system, Robot – weapon, Firing stability*

1. INTRODUCTION

In modern warfare, combat robots and unmanned gro–und vehicles (UGVs) are playing an increasingly im–portant role. These systems can operate in harsh envi–ronments, urban areas, and other high-risk situations where human deployment is hazardous. Rather than replacing soldiers, combat robots are primarily intended to reduce risks to personnel while enhancing operational effectiveness and extending battlefield capabilities. Owing to their mobility, stealth, and reliability, combat robots are regarded as a new generation of military systems. Many defense researchers have even described them as representing the third major revolution in warfare, following the introduction of gunpowder and nuclear weapons. A wide variety of combat robots have been developed worldwide. Representative examples include the MAARS robot used by the U.S. Marine Corps, which is equipped with an M240 machine gun carrying 400 rounds of ammunition and can operate continuously for 3–12 hours, and the Talon Sword robot equipped with a four-tube M202A1 grenade launcher. As combat robotic platforms continue to evolve, rese–arch has increasingly focused on the dynamic behavior of weapon systems mounted on mobile platforms.

Recent studies have developed dynamic models that more accurately represent the firing conditions of weapon systems mounted on mobile vehicles. In [1], the weapon was assumed to be rigidly mounted on the top of a flexible support, while the base of the support was rigidly connected to the vehicle body. The suspension system was modeled as linear springs and dampers, and each wheel was represented as a lumped mass supported by a linear tire spring. The robot was assumed to remain stationary during firing. The dynamic response of the system was analyzed using the finite element method. However, since the analysis was restricted to a two-dimensional firing plane, the complex three-dimensional vibration characteristics and dynamic interactions of the robot–weapon system during firing could not be fully described. Balla et al. [2,3] developed a planar dynamic model of an automatic weapon mounted on a tracked vehicle, consisting of three main components: the gun barrel, the turret, and the elevation mechanism. All rigid bodies were connected through spring–damper ele–ments. Their study demonstrated that the vibrations of the gun barrel and the elevation mechanism are the pri–mary factors affecting the firing stability of the system. In [3], the numerical results were successfully validated through experimental testing. Nevertheless, the opera–tion of the weapon's automatic mechanism during firing was not considered. Furthermore, the influence of the elastic properties of the supporting ground was negle–cted, and the vibration analysis was restricted to a single plane. In [4], a dynamic model of a robot–weapon sys–tem consisting of a weapon mounted on a four-wheeled robotic vehicle with nine degrees of freedom was deve–loped. The model included two degrees of freedom for the weapon and seven degrees of freedom for the robo–tic vehicle. The suspension system was represented by linear springs with stiffness k. Numerical simulations based on the Runge–Kutta method focused primarily on evaluating the influence of a magnetorheological dam–

Received: June 2026, Accepted: July 2026
Correspondence to: Dang Ba Ngoc
University of Defence,
Kounicova 156/65, CZ-662 10 Brno, Czech Republic
E-mail: bangoc.dang@unob.cz
doi: 10.5937/fme2603564N

per on the vibration amplitude of the system. Further–more, only single-shot firing in the firing plane was considered. The effects of the elastic characteristics of the supporting ground and the operation of the weapon's automatic mechanism were not included in the analysis.

Studies [5–7] investigated and evaluated the vib–ration characteristics of weapon launch platforms mou–nted on wheeled combat vehicles. In these models, the tires were represented as viscoelastic elements subjected to longitudinal forces, lateral forces, and self-aligning moments. The governing differential equations of moti–on were formulated based on Newton's laws of motion [6], and experimental validation was reported in [5,6]. However, these models are primarily applicable to multiple-launch rocket systems and similar artillery platforms. In contrast, automatic weapons exhibit more complex kinematic and dynamic characteristics, requ–iring a more comprehensive analysis to accurately identify all force components responsible for the system vibrations. Therefore, a comprehensive investigation of the dynamics of the robot–weapon system is essential for developing physical and mathematical models ca–pable of describing the vibration behavior of the multi–body system, as well as evaluating the firing stability and firing accuracy of the weapon system. More recently, multibody dynamic models based on the Lag–range formulation have been developed to investigate the vibration characteristics of weapon systems mounted on combat vehicles [8–10]. These studies demonstrated that the dynamic response of the weapon–vehicle system has a significant influence on firing stability and shooting accuracy. Nevertheless, the automatic firing mechanism was either neglected or simplified, and comprehensive experimental validation of the proposed models was generally lacking.

Driven by the evolving requirements of modern warfare, combat robots are expected to play an incre–asingly important role in future military operations. Ad–vances in artificial intelligence, sensing technologies, and remote-control systems have enabled combat robots to perform a wide range of missions, including recon–naissance, fire support, and direct combat. Compared with human soldiers, combat robots can operate conti–nuously with high precision under hazardous conditions while significantly reducing risks to personnel. For weaponized combat robots, firing stability is one of the key factors governing shooting accuracy and target engagement capability. Consequently, understanding the dynamic behavior of the robot–weapon system under firing excitation is essential for improving firing performance. Accurate dynamic modeling not only provides insight into the vibration mechanisms that degrade firing stability but also establishes a theoretical foundation for the structural design, parameter optimization, and control of combat robot systems.

In this study, the dynamic behavior of a combat robot equipped with a gas-operated small-caliber automatic weapon is investigated under firing excitation. Unlike previous studies, the proposed model explicitly considers the coupled interaction between the operation of the automatic firing mechanism and the vibration response of the robot–weapon system. In addition, the influence of ground compliance is incorporated into the dynamic analysis to more accu–rately represent practical firing conditions. The auto–matic firing mechanism is a key subsystem of an auto–matic weapon, and its kinematic characteristics have a direct influence on the dynamic response and firing stability of the entire robot–weapon system. Therefore, the mutual interaction between the firing mechanism and the structural vibration of the robot is taken into account throughout the firing cycle. A BREN 2 assault rifle manufactured in the Czech Republic was selected as the weapon platform because of its high operational reliability and modular design, which allows the use of different calibers. Experimental firing tests were con–ducted using 5.56×45 mm SS109 ammunition to deter–mine the motion characteristics of the bolt carrier and to measure the principal vibration responses of the robot in the firing plane. The experimental results were subse–quently used to validate the proposed dynamic model.

2. PROBLEM STATEMENT

2.1 Modeling Assumptions

To establish the dynamic model of the robot–weapon system in three-dimensional space, the following assu–mptions are adopted:

- The wheeled combat robot is assumed to remain stationary during firing. The elevation angle and azimuth angle are kept constant; therefore, target tracking is not considered.
- The wheels are modeled as linear springs acting only in the vertical direction. In the longitudinal direction, the wheels are assumed to possess sufficiently high stiffness, thereby preventing any longitudinal displacement of the vehicle body. Based on the above assumptions, the vehicle body is also assumed to have no rotational motion about the vertical Z-axis (Figure 1), since such rotation would induce longitudinal displacement of the wheels, which is neglected in the present model.

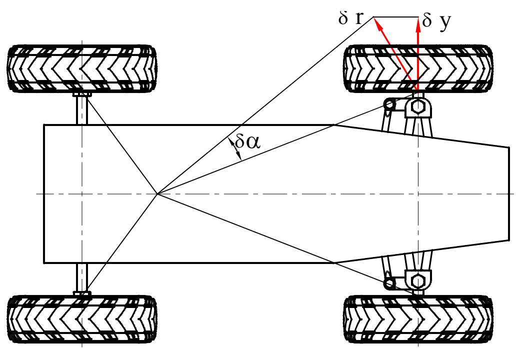

Figure 1. Scheme of the vehicle body rotating about the Z-axis by an angle $\delta\alpha$.

- The supporting ground is assumed to be flat and ho–mogeneous. Its elastic, viscous damping, and frictio–nal properties are assumed to act uniformly on all whe–els. These effects are represented by equivalent spring–damper elements associated with each wheel assembly.
- The entire robot body, elevation mechanism, azi–muth mechanism and the weapon are considered as homogeneous objects, symmetrical about its sym–metry axes.

– All joints and mechanical connections between the system components are assumed to be perfectly rigid, with no structural deformation or joint clea–rance during operation.

For the automatic weapon mounted on the robot, the bolt carrier is regarded as the primary moving compo–nent that drives the operation of the other mechanisms, including bolt locking and unlocking, cartridge feeding, cocking, and cartridge case extraction and ejection. During firing, the firing force (F_{fos}) acts on the robot–weapon system along the longitudinal axis of the barrel.

The robot–weapon system is modeled as a multi–body dynamic system consisting of five rigid bodies (Figure 2). Body 1 represents the robot platform, with mass m_1 and center of mass located at O_1. Body 2 denotes the yaw rotation mechanism, with mass m_2 and center of mass at O_2. Body 3 represents the pitch rotation mechanism, with mass m_3 and center of mass at O_3. Body 4 corresponds to the gun body, with mass m_4 and center of mass at O_4. Body 5 represents the bolt carrier of the automatic firing mechanism, with mass m_5 and center of mass at O_5.

In addition, the dynamic model incorporates the in–ternal components of the automatic operating mecha–nism, in which the motion of the bolt carrier (body 5) is transmitted to other moving components through the corresponding mechanical linkages. Each component of the automatic mechanism is represented by an equi–valent reduced mass m_i', considering the transmission ratio K_i and mechanical efficiency η_i. The equivalent inertial properties of these components are included in the dynamic equations to accurately describe the inte–raction between the automatic firing mechanism and the overall robot–weapon system during the firing process.

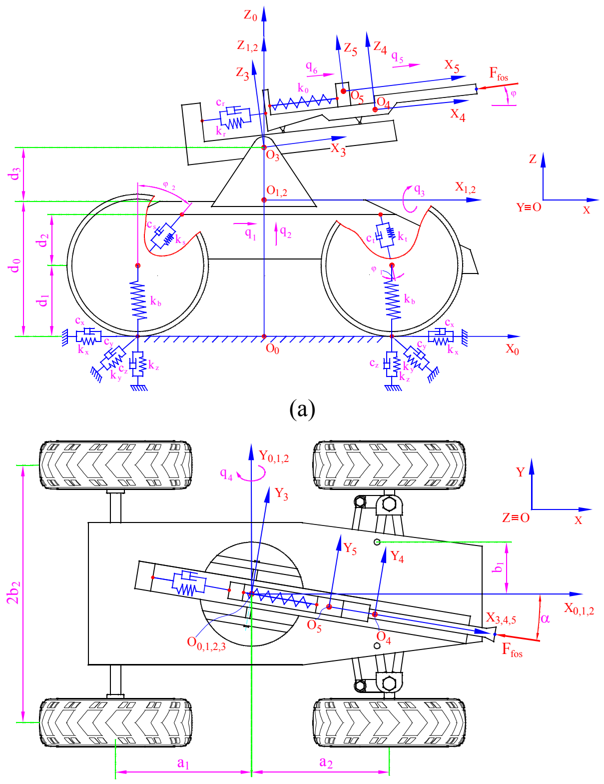

Figure 2. Robot–weapon system in combat state: (a) side view, (b) top view.

To observe and analyze the mechanical system, it is first necessary to establish an inertial reference frame $O_0X_0Y_0Z_0$ attached to the ground (considered as object 0), denoted as $R_0 = (O_0X_0Y_0Z_0)$: The origin O_0 is defined as the intersection of the turret rotation axis with the ground plane. The X_0 - axis is oriented forward and is defined as the intersection of the vehicle body's symmetry plane with the ground plane. The Z_0 - axis coincides with the turret rotation axis and is oriented vertically upward. The Y_0 - axis is determined so that it, along with the X_0 - axis and Z_0 - axis forms a right-handed coordinate system (a right-handed triad) $X_0Y_0Z_0$. $R_k = (O_kX_kY_kZ_k)$: accounts for the local coordinate system established at the k-th solid, $k = 1,\dots,5$. From the assumptions and layout of objects, the combat vehicle robot system has 6 independently generalized coordinates (DOF): $[q_j]=[q_1, q_2, q_3, q_4, q_5, q_6]$, where q_1 - longitudinal displacement of body 1 along X_0 - axis; q_2 - longitudinal displacement of body 1 about Z_0 - axis; q_3 - angular displacement of body 1 about X_0 - axis; q_4 - angular displacement of body 1 about Y_0 - axis; q_5 - longitudinal displacement of body 4 along X_3 – axis; q_6 - longitudinal displacement of body 5 along X_3 – axis.

2.2 Establishment of the Mathematical Model

Several dynamic modeling and stability analyses of automatic weapons [11-13] and weapons mounted on combat vehicles [14] have also employed the Lagrange method. For the weapon-robot mechanical system, the differential equations governing the vibrations can be written in the following form:

$$\frac{d}{dt}\left(\frac{\partial T^{\Sigma}}{\partial \dot{q}_j}\right)-\frac{\partial T^{\Sigma}}{\partial q_j}+\frac{\partial \Pi^{\Sigma}}{\partial q_j}+\frac{\partial D^{\Sigma}}{\partial \dot{q}_j}=Q_j . \tag{1}$$

where $T^{\square}$ (kg·m^2/s^2) is total kinetic energy of the whole mechanical system ; $\Pi^{\square}$ (kg·m^2/s^2) is the potential energy function of the force elements that possess potential energy; $D^{\square}$ is the dissipation function, corresponding to the resistive force components in the system; Q_j is the generalized force vector acting on the mechanical system; q are the generalized coordinate; j is the degree of freedom of the system, $j = 1,\dots,6$.

Kinetic energy of the mechanical system:

$$T^{\Sigma}=\frac{1}{2}\sum_{k=1}^{5}\left(\dot{R}_k^T M_k \dot{R}_k+\bar{\omega}_k^T A_0^k I_k A_0^{kT}\bar{\omega}_k\right) \tag{2}$$

where R_k is the center of mass vector of body k in the fixed coordinate system O_0; M_k is mass matrix of body k; $\bar{\omega}_k$ is the angular velocity vector of the body k represented on the fixed coordinate O_0; A_0^k is transfer matrix from system O_k to system O_0; A_0^{kT} is the inverse matrix of the matrix A_0^k; I_k is matrix of the inertia tensor of the body k to the axis system O_k.

Potential energy of mechanical system:

The potential energy of the system consists of the gravitational potential energy and the elastic potential energy stored in the equivalent spring elements repre–

senting the suspension system, as well as in the viscoelastic elements modeling the stiffness of the supporting ground and the tires.

Gravitational potential energy:

$$\Pi_1 = \sum_{i=1}^{5} g m_i r_i(z) . \tag{3}$$

where g is the acceleration due to gravity (g = 9.81 m/s^2), m_i is the mass of the i-th object, r_i is the matrix determining the coordinates of the i-th object's center of gravity with respect to the reference frame O_0.

The elastic potential energy of the connecting ele– ments is expressed as follows:

$$\Pi_2 = \frac{1}{2}\sum_j K_j \left(\Delta l_j\right)^2 . \tag{4}$$

where K_j is the stiffness of the j-th elastic element; Δl_j is the deformation (elongation or compression) of the j-th elastic element.

Total potential energy of the multibody system:

$$\Pi^{\Sigma} = \Pi_1 + \Pi_2 . \tag{5}$$

Dissipation function:

The viscoelastic elements in the model, including the suspension spring–damper units and the tires, cont– ribute linear damping forces represented by Rayleigh's dissipation function:

$$D^{\Sigma} = \frac{1}{2}\sum_j c_j \left(\Delta i_j\right)^2 . \tag{6}$$

where: c_j is the viscous damping coefficient of the j-th viscoelastic element; Δi_j is the deformation rate (relative deformation velocity) of the j-th viscoelastic element.

Potential work and generalized force:

Consider the potential work of the generalized force F_k and moment M_k, see in [11], [13-15]:

$$\delta W_1 = \sum_{j=1}^{6}\left[\sum_{k=1}^{5} F_k^T \frac{\partial R_k}{\partial q_j}\right]\delta q_j . \tag{7}$$

$$\delta W_2 = \sum_{j=1}^{6}\left[\sum_{k=1}^{5} M_k^T \frac{\partial \theta_k}{\partial q_j}\right]\delta q_j . \tag{8}$$

where δW_1 is the virtual work produced by the force F_k; δW_2 is the virtual work produced by the moment M_k.

If the connections in the mechanical system are considered ideal, ignoring frictional forces, then the generalized force Q_j is determined as formula:

$$Q_j = \sum_{k=1}^{5} F_k^T \frac{\partial R_k}{\partial q_j} . \tag{9}$$

$$Q_j = \sum_{k=1}^{5} M_k^T \frac{\partial \theta_k}{\partial q_j} . \tag{10}$$

where Q_j is the generalized force corresponding to the generalized coordinates q_j; F_k and M_k are the force and moment acting on the k-th object, respectively.

After determining the kinetic energy, potential energy, Rayleigh's dissipation function, and generalized forces of the multibody system, the partial derivatives with respect to the generalized coordinates and gene– ralized velocities are evaluated and substituted into Eq. (1). Consequently, the governing system of differential equations describing the vibration of the robot–weapon system is obtained as follows:

$$M(q)\ddot{q} + C(q,\dot{q})\dot{q} + K(q) = Q(q,t) . \tag{11}$$

where $M(q)$ is the generalized mass matrix of the mul– tibody system; $C(q,\dot{q})$ is the vector of nonlinear iner– tial forces; $K(q)$ is the vector of equivalent elastic for– ces; $Q(q, t)$ is the vector of generalized forces due to external loads.

The above system consists of six nonlinear differe– ntial equations, which fully describe the vibration beha– vior of the robot–weapon multibody system during firing.

2.3 Ground Stiffness and Viscous Damping Characteristics

To achieve a more realistic simulation of the actual firing conditions of combat robots, one of the suitable approaches is to model the supporting ground as a viscoelastic system, which is equivalent to a spring element with stiffness k and a damper with viscous damping coefficient c. Depending on the direction of motion and the type of ground conditions, these parameters are determined using different formulations and corresponding values. In this study, the coefficients k_x, k_y, and k_z, as well as c_x, c_y, and c_z, are assumed to represent the stiffness and viscous damping coefficients of the ground in the three coordinate directions, respectively (Figure 2a). The influence of ground properties along different directions has been investigated by several researchers in [16–19]. The equations used to determine the elastic stiffness and viscous damping coefficients of the supporting ground are given as follows [19]:

The elastic stiffness and viscous damping coeffi– cients in the vertical direction (OZ):

$$k_z = \frac{4.E_0.b}{1-\nu} . \tag{12}$$

$$c_z = 3.4 \times \frac{b^2}{1-\nu}.\sqrt{E_0.\rho} . \tag{13}$$

The elastic stiffness and viscous damping coefficients in the horizontal direction (OX, OY):

$$k_x = k_y = \frac{32.(1-\nu)}{7-8.\nu} E_0.b . \tag{14}$$

$$c_x = c_y = 0.576 \times \frac{32.(1-\nu)}{7-8.\nu}.\sqrt{E_0.\rho} . \tag{15}$$

where ρ is the ground density; b (m) is the tire width; and E_0 (Pa) is the Young's modulus of the supporting ground.

2.4 Analyze the Forces Acting on the Robot

Force exerted by the wheel:

F_{wfr}, F_{wfl}, F_{wrr} and F_{wrl} are the tire forces at front right, front left, rear right and rear left, respectively. They are determined by the following formula:

$$F_{\mathrm{w}} = k_c\,(x_{0\mathrm{w}} + \delta x_{\mathrm{w}})\,. \qquad (16)$$

where, x_{0w} is the initial compression of tires springs; δx_w is the deviation of the elastic element vector of the tire□replacement spring; k_c is the substitute stiffness factor of the elastic component connection series mode–lling the rubber tire and the elastic components mode–lling the ground.

According to [20], the equivalent deformation of the tire–ground system δ_c is expressed as follows:

$$\delta_c = \delta_t + \delta_g\,. \qquad (17)$$

where δ_t is the tire deformation; δ_g is the ground defor–mation.

These deformations are nonlinear [20], therefore:

$$F = k_c\,\delta_c^{3/2}\,. \qquad (18)$$

where F is the gravitational force of the wheel acting on the ground in the vertical direction.

From equations (17) and (18), the equivalent stiff–ness coefficient k_c is determined as follows:

$$k_c = \frac{k_b\,k_z}{\left(k_b^{\frac{2}{3}} + k_z^{\frac{2}{3}}\right)^{\frac{3}{2}}} \qquad (19)$$

where k_b (N/m) is the rubber band stiffness.

Whereas the rubber band stiffness with the following expression [21]:

$$k_b = \frac{\sqrt{32}\,E\,b\sqrt{r_1}}{3h}\,. \qquad (20)$$

where E (Pa) is the Young module for rubber, h (m) is the rubber band height, b (m) is the rubber band width, r_1 (m) is the wheel radius along with band.

Suspension system force:

The combat robot has three suspension systems: two front suspensions distributed symmetrically across the firing plane, and one rear suspension lying in the firing plane. The forces are calculated as:

$$\begin{aligned} F_a &= 2k_t(\Delta l_t - \Delta l_{0t})\cos\varphi_1 + 2c_t\,\dot{\Delta l}_t \\ &\quad + k_s(\Delta l_s - \Delta l_{0s})\cos\varphi_2 + c_s\,\dot{\Delta l}_s \end{aligned}\,. \qquad (21)$$

where: k_t (N/m), k_s (N/m) are the stiffness of the front and rear suspension springs; Δl_t (m), Δl_s (m) are the current compression of the front and rear springs; Δl_{0t} (m), Δl_{0s} (m) are the initial compression of the front and rear sp–rings at equilibrium; c_t (N.s/m), c_s (N.s/m) are the viscous damping coefficients of the front and rear suspensions.

The gravitational force:

The gravitational force acting on the k-th rigid body is applied at its center of mass, perpendicular to the horizontal plane and directed vertically downward:

$$P_k = m_k\,g\,. \qquad (22)$$

The force of shot:

The firing force (F_{fos}) acting on the weapon and causing the motion of its components depends on the operating principle of the weapon, as reported in [22–24]. For small-caliber automatic weapons operating based on the gas-operated principle, the definition and analysis of the forces acting on the weapon are described in [22]. The force components include:

F_H – the force generated by the propellant gas pressure acting on the breech face;

F_{TP} – the force generated by the propellant gas pressure acting on the front wall of the gas chamber;

F_{PP} – the elastic force of the return spring acting on the weapon receiver;

F_{RZP} – the impact force between the bolt carrier and the rear wall of the receiver;

F_{RPP} – the impact force between the bolt and the front wall of the receiver.

$$F_\Sigma = F_H - F_{TP} + F_{RZP} + F_{PP} - F_{RPP}\,. \qquad (23)$$

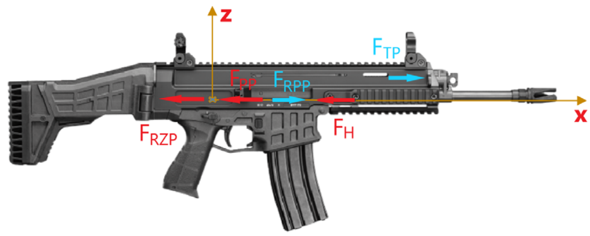

Figure 3. Forces acting on the mount of the BREN 2.

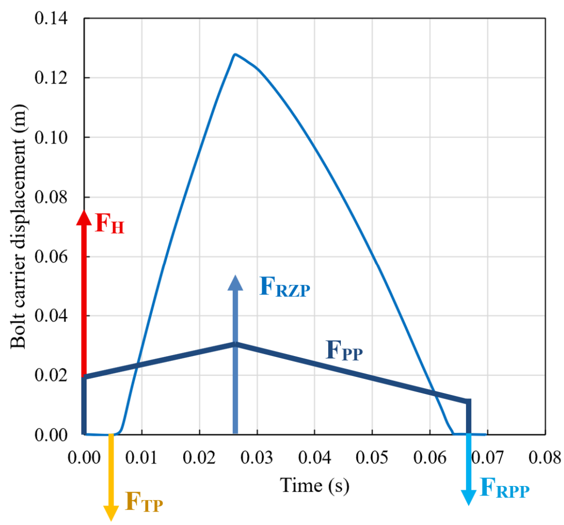

Figure 4. Diagram of forces acting on the BREN 2 rifle.

To determine these force components, it is necessary to solve the internal ballistics problem, the gas chamber thermodynamic problem, and the dynamics of the auto–matic mechanism. Figures 3 and 4 illustrate the direc–tions of action of the individual forces. These forces act on the weapon receiver during a functional cycle, and their resultant is transmitted from the weapon to the robot, inducing the motion of the entire robot–weapon system. During burst firing, these forces exhibit periodic characteristics.

The force components are determined as follows:

Force generated by the propellant gas pressure ac–ting on the breech face:

To determine the force generated by the propellant gas pressure p acting inside the barrel, the internal ballistics problem must be solved. For a gas-operated automatic weapon, the system of differential equations describing the internal ballistics process presented in [25] is employed.

The force generated by the propellant gas pressure acting on the breech face F_H is determined as follows:

$$F_H = S.p(t)\,. \tag{24}$$

where S (m^2) is the cross-sectional area of the barrel bore; $p(t)$ (Pa) is the propellant gas pressure acting on the breech face, which is determined by solving the internal ballistics equations.

The total impulse of the propellant gas pressure inside the barrel is calculated as formula:

$$I_1 = I_{01} + I_{02}\,. \tag{25}$$

where I_{01} is the impulse of the propellant gas pressure during the projectile motion inside the barrel; and I_{02} is the impulse of the propellant gas pressure during the final stage of the propellant gas action.

$$I_{01} = \int_0^t F_H(t)\,dt = S\int_0^t p(t)\,dt\,. \tag{26}$$

where t (s) is time of projectile motion inside the barrel.

$$I_{02} = S\int_0^\tau p_{0t}\,dt = S\int_0^\tau p_{00}\,e^{-bt}dt\,. \tag{27}$$

where: p_{ot} (Pa) is the propellant gas pressure acting on the breech face at time t; p_{oo} (Pa) is the propellant gas pressure acting on the breech face at the moment the projectile exits the barrel (t = 0); b is the Bravin coef–ficient; τ is the final action duration of the propellant gases acting on the barrel, determined according to the Bravin law.

$$\tau = \frac{1}{b} Ln \frac{p_{00}}{p_{0\tau}}\,. \tag{28}$$

where $p_{0\tau}$ (Pa) is the propellant gas pressure on the breech face at the end of the final action phase.

The force acting on the gas piston system:

The BREN 2 rifle is a gas-operated automatic weapon, in which the gas operating system serves as the energy source for the automatic mechanism. The pro–pellant gases are diverted from the barrel through a gas port located on the barrel wall into the gas chamber, where they act on the piston face and drive the bolt carrier into motion. To determine the variation law of the gas pressure in the gas chamber, the internal bal–listics equations and the gas chamber thermodynamic equations presented in [26] are solved simultaneously.

The force generated by the propellant gas pressure acting on the front wall of the gas chamber F_{TP} is deter–mined as follows:

$$F_{TP} = p_b\,S_b\,. \tag{29}$$

where p_b (Pa) is the gas pressure inside the gas chamber, and S_b (m^2) is the cross-sectional area of the gas chamber.

The impulse generated by the propellant gas pres–sure in the gas chamber is calculated as follows:

$$I_2 = \int_{t_\phi}^{t_d} F_{TP}(t)\,dt\,. \tag{30}$$

where t_{ϕ} (s) is the time for the projectile to travel past the gas port; t_d (s) is the projectile travel time inside the barrel.

The force generated by the return spring:

In automatic weapons, the rate of spring deformation is lower than the propagation velocity of the shock wa–ve; therefore, the return spring force can be calculated using the following equation:

$$F_{PP} = \Pi_0 - k_0.X\,. \tag{31}$$

where Π_0 (N) is the initial compression force of the return spring; k_0 (N/m) is the spring stiffness; X (m) is the total rearward travel of the bolt carrier.

The impact force between the bolt carrier and the re–ar wall of the receiver at the end of the rearward stroke:

$$F_{RZP} = m_5(V_{50} - V_5)\,/\,dt\,. \tag{32}$$

where V_{50} (m/s) and V_5 (m/s) are the velocities of the bolt carrier before and after the impact, respectively.

$$F_{RPP} = m_5\,V_5^{'}\,/\,dt\,. \tag{33}$$

where $V_5^{'}$ (m/s) is the velocity of the bolt carrier at the end of the forward stroke.

The velocities of the bolt carrier are determined by solving the automatic mechanism dynamics problem of the BREN 2 rifle.

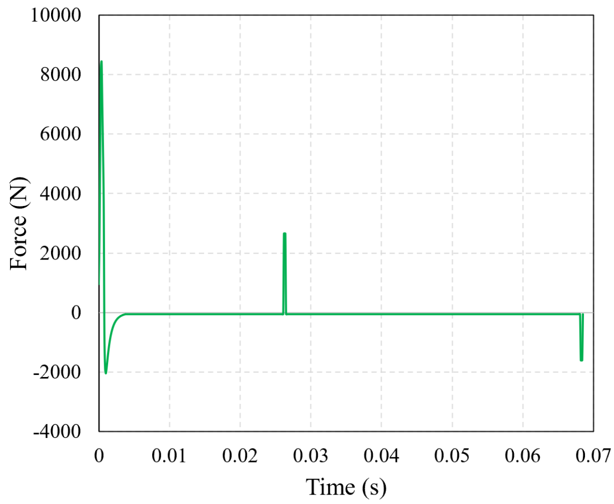

Figure 5. Diagram of the total impulse acting on the BREN 2 rifle during one operating cycle.

Figure 5 presents the time history of the total force acting on the robot due to the BREN 2 rifle firing a 5.56×45 mm SS109 cartridge during a complete ope–rating cycle. The return spring force F_{PP} does not signi–ficantly affect the motion of the entire weapon system because its magnitude is relatively small and insuf–ficient to overcome the friction forces in the guide rails of the elevation mechanism.

3. CALCULATION RESULTS

The main input parameters (PS0) for solving the system of differential equations (10) include the stiffness and damping parameters of the elastic-damping elements, as well as those of the supporting ground, are presented in Table 1. The structural parameters of the robot, which are presented in Table 2.

Table 1. The parameters of elasticity and viscous resistance

Parameters	Symbol	Value
The stiffness coefficient of the springs replacing the wheels	k_b	(18000–20000) N/m
The stiffness coefficient of the springs replacing the front suspension system	k_t	(1200–1300) N/m
The stiffness coefficient of the springs replacing the rear suspension system	k_s	(1500–1600) N/m
The damping coefficient of the dampers replacing the front suspension system	c_t	(300–350) Ns/m
The damping coefficient of the dampers replacing the rear suspension system	c_s	(400–450) Ns/m
Coefficient elastic of the background in the X-direction	k_x	(250–350) N/m
Coefficient elastic of the background in the Y-direction	k_y	(250–350) N/m
Coefficient elastic of the background in the Z-direction	k_z	(450–520) N/m
Drag coefficient viscous of the background in the X-direction	c_x	(1–1.5) N□s/m
Drag coefficient viscous of the background in the Y-direction	c_y	(1–1.5) N□s/m
Drag coefficient viscous of the background in the Z-direction	c_z	(2–3) N□s/m

Table 2. Structural parameters

Body	Mass (kg)	J_x (kg.m^2)	J_y (kg.m^2)	J_z (kg.m^2)
1	110	1.8195	4.6829	5.8973
2	5.73	0.0183	0.0184	0.0144
3	3.85	0.023	0.025	0.034
4	3.16	0.00042	0.0127	0.0093
5	0.395	0.0088	0.0089	0.00058

These structural parameters are determined using Autodesk Inventor 3D modeling software based on the geometric model of the robot body (Figure 6).

The solution of the internal ballistics problem provides the time-dependent variation of the propellant gas pressure inside the barrel, as shown in Figure 7, and the projectile velocity during its motion inside the barrel, as shown in Figure 8.

The internal ballistic calculation results for the 5.56×45 mm SS109 ammunition fired from the BREN 2 assault rifle with an 11-inch barrel show good agree–ment with the data reported by the manufacturer. Speci–fically, the calculated maximum chamber pressure is 347.11 MPa (Figure 7), which is close to the measured chamber pressure of 350 MPa obtained from pressure tests of a 5.56×45 mm SS109 test barrel, corresponding to a relative error of only 0.82%.

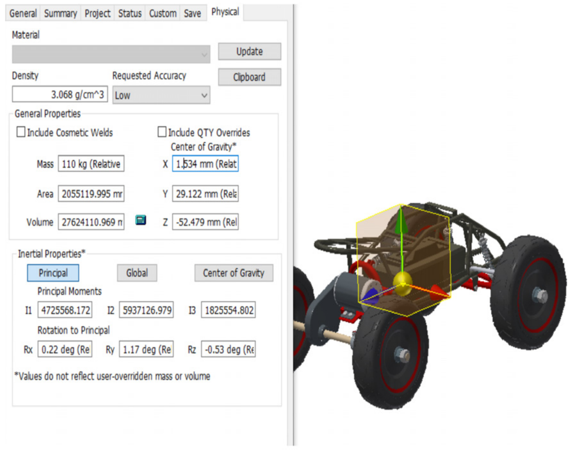

Figure 6. Input parameters obtained from Autodesk Inventor.

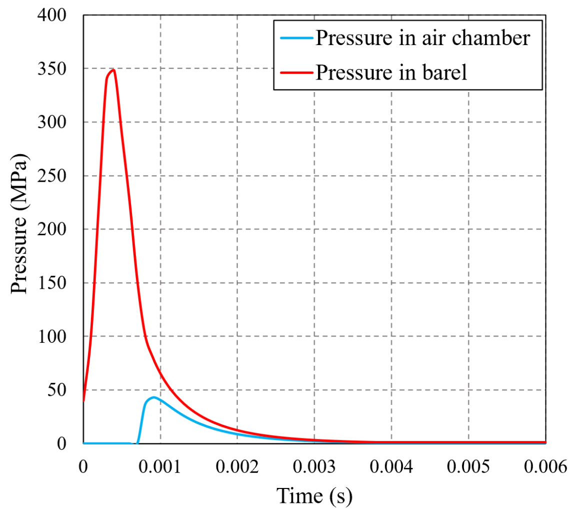

Figure 7. Pressure in the barel and gas chamber.

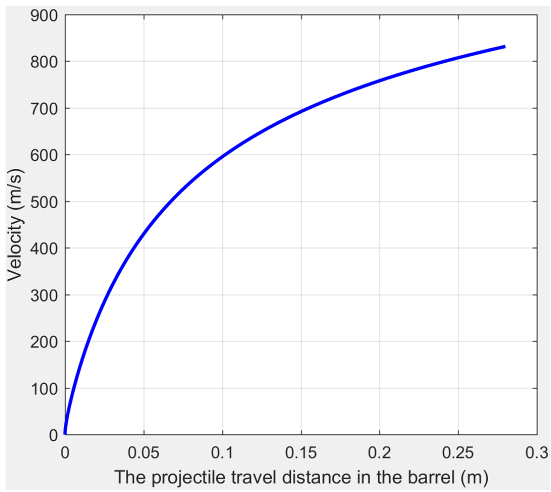

Figure 8. Projectile velocity.

Furthermore, the calculated muzzle velocity is 865.93 m/s (Figure 8), compared with the manufacturer-reported value of 870 m/s, resulting in a relative error of 0.47%. These results demonstrate that the proposed internal ballistic model can accurately predict the main ballistic characteristics of the ammunition–weapon system and provide reliable input parameters for subsequent dynamic analysis of the robot–weapon system during firing.

The calculated firing cycle duration is 0.0685 s, corresponding to a theoretical cyclic rate of 876 rounds /min. This value is in good agreement with the firing rate reported in [27], which is 850 ± 100 rounds/min, resulting in a relative error of 3.06%. The comparison confirms the accuracy of the proposed model in predicting the operating characteristics of the automatic firing mechanism.

To determine the kinematic behavior of the bolt carrier of the BREN 2 rifle during the firing process, a high-speed motion measurement system based on a MotionXtra HG-100K camera was employed. The camera was configured with a recording rate of 9000 frames/s to capture the bolt carrier motion with high temporal resolution. During the experiment, the rifle was rigidly mounted on a dedicated STZA-12 firing test bench to ensure stable mounting conditions and minimize the influence of external vibrations. The image acquisition process was automatically triggered by an acoustic sensor that detected the sound generated during firing. The schematic configuration of the experimental setup is presented in Figure 9.

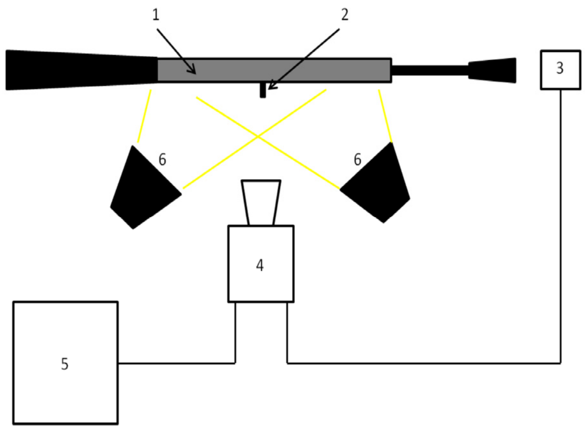

Figure 9. Schematic diagram of the experimental setup: (1) Weapon; (2) Bolt carrier charging handle; (3) Trigger unit; (4) High-speed camera; (5) Computer; (6) Lighting system.

The dynamic analysis of the BREN 2 rifle automatic mechanism was performed to determine the motion characteristics of the bolt carrier. The calculated results of the bolt carrier displacement and velocity responses are presented in Figures 10a and 11a, respectively.

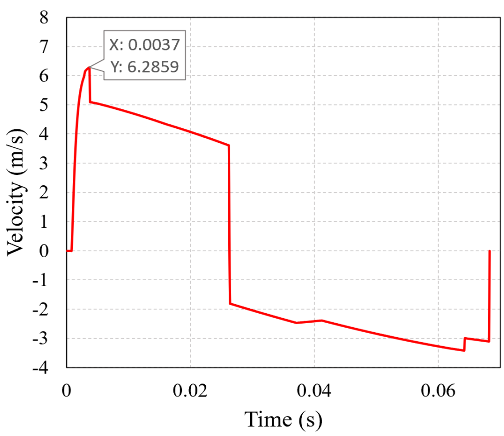

(a) theoretical results

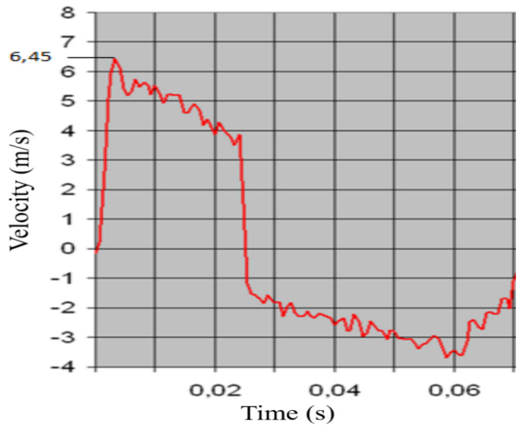

(b) experimental results

Figure 10. Motion velocity of the base body.

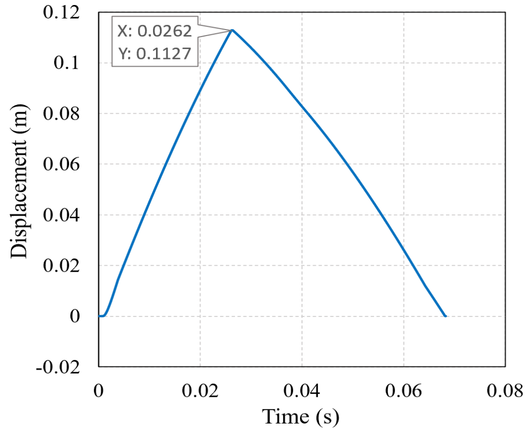

(a) theoretical results

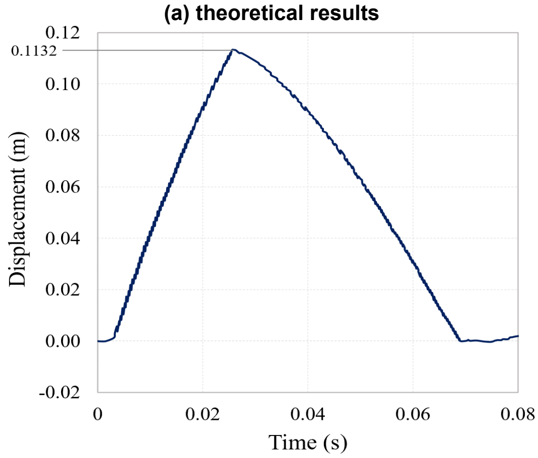

(b) experimental results

Figure 11. Displacement of the base body $q_6(t)$.

The theoretical analysis predicts that the maximum bolt carrier velocity is 6.286 m/s (Figure 10a), while the corresponding maximum recoil displacement is 0.1127 m (Figure 11a). The experimental results obtained from the BREN 2 rifle (Figures 10b and 11b) show good agreement with the theoretical predictions. Specifically, the measured maximum bolt carrier velocity is 6.45 m/s (Figure 10b), corresponding to a relative error of 2.54% compared with the theoretical result. Likewise, the measured maximum recoil displacement is 0.1132 m (Figure 11b), with a relative error of 3.79%.

The comparison results demonstrate that the proposed theoretical model provides reliable predictions and can therefore be confidently employed for subsequent analyses of the firing stability of the robot–weapon system.

To further investigate the vibration behavior of the robot during firing, several key parameters were selected as evaluation criteria for the firing stability, and reliability of the robot–weapon system. These parameters include the translational displacements of the robot and its angular vibrations in the vertical and horizontal planes. The simulation results for an elevation angle and an azimuth angle of 15° under both single-shot and three-round burst firing modes are presented in Figures 12 and 13.

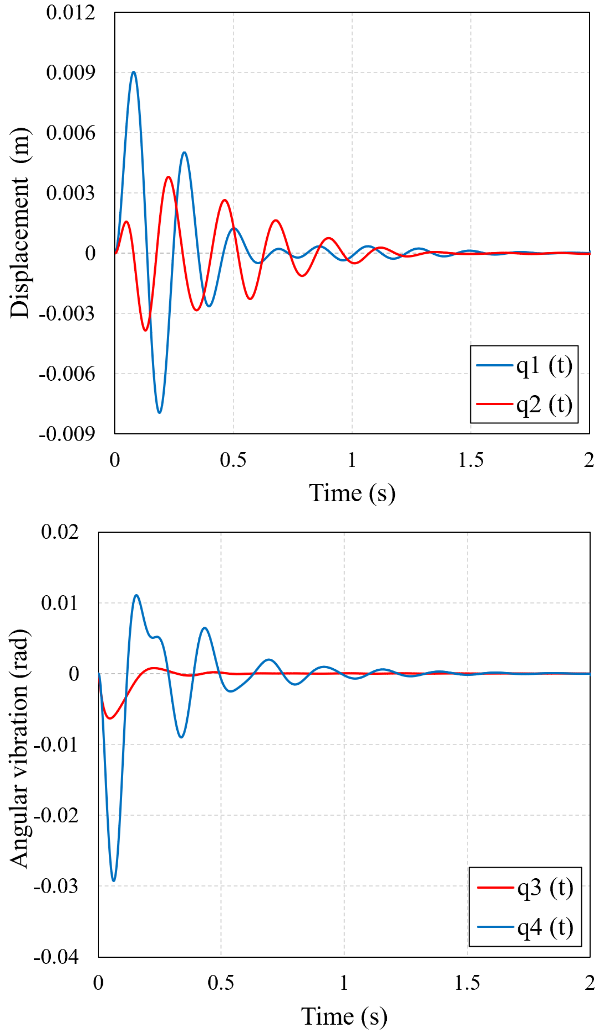

Figure 12. Single-shot firing.

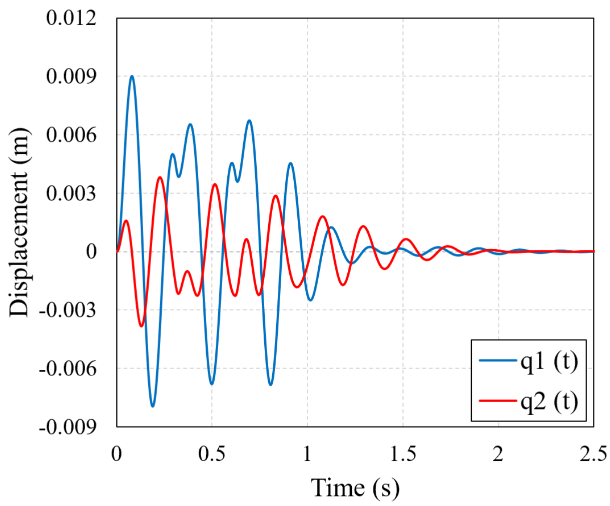

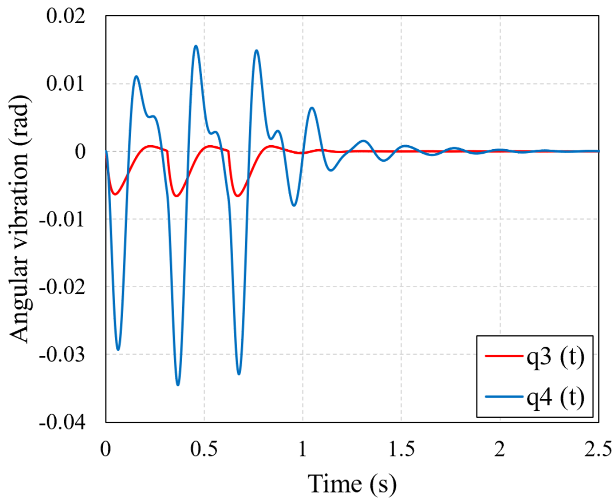

Figure 13. Three-round burst firing.

Under firing excitation, including both single-shot and three-round burst firing modes, the robot exhibits distinct vibration characteristics along different degrees of freedom. The translational vibration along the X-axis (q_1) contributes primarily to the azimuth error α, whereas the translational vibration along the Z-axis (q_2) directly affects the elevation error φ. urthermore, the angular displacement about the Y-axis (q□) is significantly greater than that about the X-axis (q□). These results indicate that the robot is more susceptible to dynamic instability in pitching motion about the Y-axis and translational motion along the X-axis under firing excitation. Such vibration characteristics degrade the firing stability of the robot and consequently reduce its shooting accuracy.

4. EXPERIMENTAL MEASUREMENT OF VIBRATIONS

The reliable operation, firing stability, and shooting accuracy of a combat robot are primarily evaluated based on the vibration response of the robot–weapon system under firing excitation. Therefore, the objective of this section is to experimentally characterize the vibration response of the robot during firing and to validate the proposed theoretical model through comparison between the experimental measurements and the numerical predictions. The experimental setup is illustrated in Figure 14. A BREN 2 assault rifle was rigidly mounted on the robot chassis through an intermediate mounting structure without any recoil attenuation mechanism. Accordingly, to ensure consistency between the experimental configuration and the theoretical model, the recoil spring in the numerical model was assumed to have infinite stiffness, corresponding to a rigid connection between the weapon and the robot. During the experiments, the firing elevation angle and azimuth angle were both set to 0°. The ambient temperature was 12 °C, and the wind speed was approximately 4 m/s.

A GoPro HERO7 Black high-speed camera, operating at a resolution of 1280 × 960 pixels and a frame rate of 240 frames/s (fps), was employed to capture the motion of the robot in the vertical plane (firing plane). The camera was rigidly mounted on a fixed support to ensure a stationary reference frame throughout the ex–

periments and to minimize the influence of external vibrations. The recorded videos were stored in MP4 format and subsequently processed using Matlab.

Figure 14. Experimental measurement of robot vibrations.

The vibration response of the robot was extracted by tracking high-contrast markers attached to the robot in successive video frames. After camera calibration, the image coordinates of the markers were converted from pixel coordinates into physical displacement coordi–nates. The resulting displacement–time histories were then used to characterize the vibration response of the robot following each firing event and to provide the experimental data for validation of the proposed dynamic model.

The vibration response of the robot subjected to single-shot firing at an elevation angle of 0° and an azimuth angle of 0° was numerically simulated using Maple. The comparison between the theoretical predic–tions and the experimental measurements is presented in Figures 15 and 16.

The experimental results show good agreement with the theoretical predictions. Specifically, the maximum vibration amplitude of the robot along the X-axis in the firing plane differs from the theoretical result by 4.73% (Figure 15), while the corresponding maximum vibration amplitude along the Z-axis exhibits a discrepancy of 6.79% (Figure 16). These results confirm the capability of the proposed dynamic model to predict the vibration response of the robot subjected to firing excitation with satisfactory accuracy.

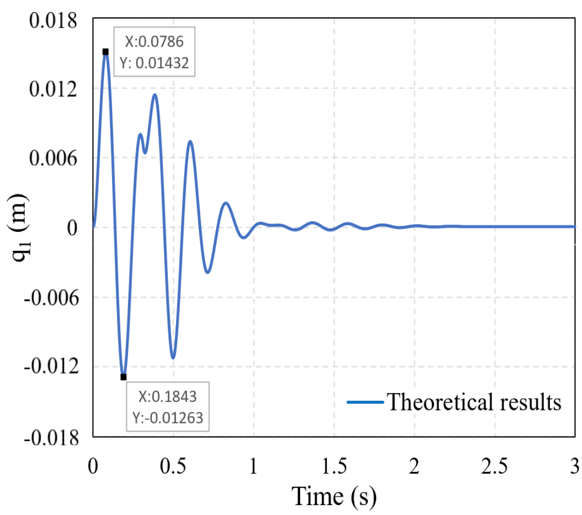

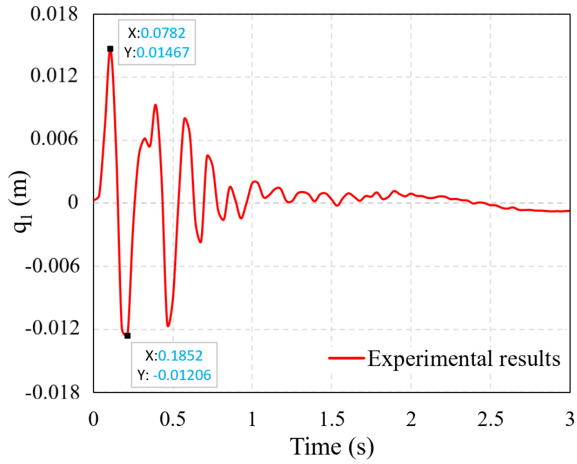

Figure 15. Robot displacement along the X-axis during firing.

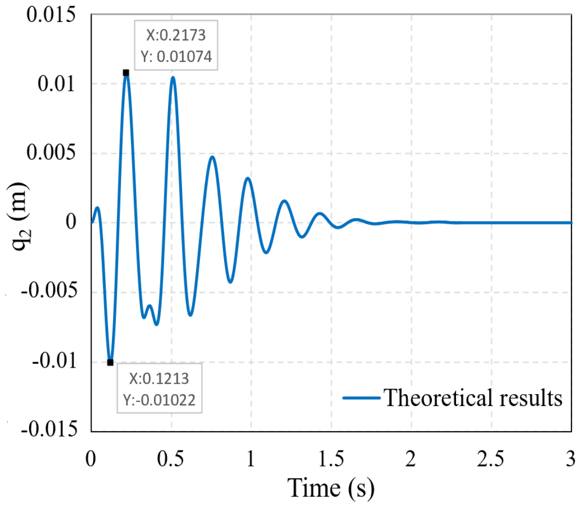

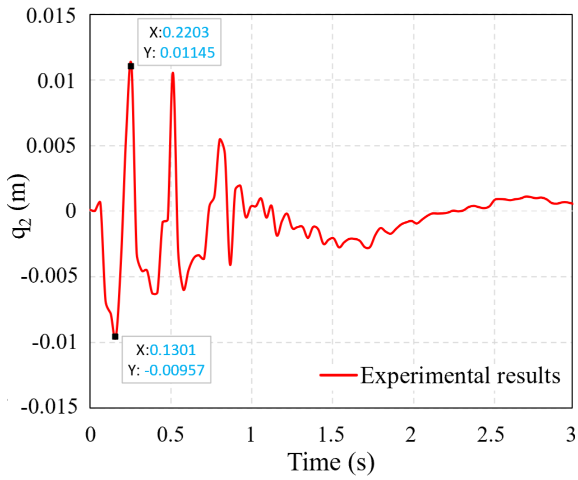

Figure 16. Robot displacement along the Z-axis during firing.

The observed discrepancies can be attributed to se–veral factors. First, the theoretical model incorporates a number of simplifying assumptions to facilitate the dyna–mic analysis. Second, the weapon is rigidly mounted on the robot chassis; therefore, the stiffness and damping parameters assigned to the connecting components may not fully represent their actual dynamic behavior under the impulsive loading generated during firing. In addition, uncertainties in system parameters, manufacturing and assembly tolerances, and experimental measurement errors may also contribute to the differences between the numerical and experimental results.

5. CONCLUSION

The dynamic model of the automatic weapon mounted on a combat robot consists of five rigid bodies and six degrees of freedom, and is formulated based on the Lagrange equations of the second kind. Numerical simulations are performed to predict the three-dimensional vibration response of the robot–weapon system under firing excitation. To validate the proposed model, the robot vibrations during firing are experimentally measured using a high-speed camera. The recorded videos are processed to extract the principal vibration components of the robot, providing reliable experimental data for comparison with the numerical predictions and thereby validating the proposed dynamic model.

The obtained results demonstrate that the proposed dynamic model provides an effective tool for evaluating the firing stability of the combat robot. By varying the key design parameters, including the stiffness and viscous damping characteristics of the elastic elements, the model enables a comprehensive assessment of their influence on the dynamic response of the robot–weapon system under firing excitation. Consequently, the proposed model can serve as a valuable tool for the design, analysis, and optimization of the robot–weapon system, contributing to improved firing stability and enhanced shooting accuracy. Future work will focus on optimizing the key structural parameters that have the greatest influence on the firing stability of the robot–weapon system. In addition, the experimental setup and validation methodology will be further refined to improve the reliability of the mathematical model and to expand its applicability under a wider range of operating conditions.

ACKNOWLEDGMENT

This paper was created with the support of the project Military Autonomous and Robotic Assets Military autonomous and robotic assets VAROPS (DZRO-FVT22-VAROPS) of the Department of weapon and ammunition, Faculty of Military Technology, University of Defence, Brno, Czech Republic.

REFERENCES

[1] Sun, H.K., Liu, Y.T. and Chen, C.G.: Dynamic analysis of a vehicular-mounted automatic weapon–planar case, Defence Science Journal, Vol. 59, No. 3, pp. 265-272, 2009, https://doi.org/10.14429/dsj.59.1520.

[2] Balla, J., Krist, Z. and Cong, I.L.: Infantry Fighting Vehicle in Case of Burst Firing, Proceedings of the International Conference on Military Technologies (ICMT 2015), Brno, Czech Republic, University of Defence, pp. 3–8, 2015.

[3] Balla, J.: Dynamics of mounted automatic cannon on track vehicle, International Journal of Mathematical Models and Methods in Applied Sciences, Vol. 5, No. 3, pp. 423–432, 2011.

[4] Nugraha, A.S., Hikmawan, M.F., Junianto, E. and Pramana, R.I.: Response of two DOF weapon system structure mounted on four wheel vehicle, Proceedings of the 2017 International Conference on Sustainable Energy Engineering and Application (ICSEEA 2017), IEEE, pp. 113–117, 2017.

[5] Bien, V.V, Phon, N.D, Dung, N.V, Phu, N.M and Minh, P.V.: Dynamic analysis of launchers on rubber tire vehicles, Journal of Defense Modeling and Simulation, 2025, https://doi.org/10.1177/15485129251326612.

[6] Van Bien, V., Macko, M., Dung, N.T., Phon, N.D., Hai, N.T. and Tuan, B.T.: Dynamic simulation analysis and optimization of firing rate of rocket launchers on wheeled vehicles, Advances in Military Technology, Vol. 16, No. 1, pp. 159–175, 2021.

[7] Konečný, P. and Nguyen, D.P.: Effect of shot duration on the firing accuracy when burst fire of unguided rockets, Proceedings of the 2021 International Conference on Military Technologies (ICMT 2021), Brno, Czech Republic, University of Defence, IEEE, pp. 1–6, June 2021.

[8] Dursun, T., Büyükcivelek, F. and Utlu, Ç.: A review on the gun barrel vibrations and control for a main battle tank, Defence Technology, Vol. 13, No. 5, pp. 353–359, 2017, https://doi.org/10.1016/j.dt.2017.06.005.

[9] Wiśniewski, A. and Rybak, P.: Stability of wheeled armoured personnel carrier firing sideways, Journal of KONES Powertrain and Transport, Vol. 26, No. 2, pp. 175–180, 2019.

[10] Tuan, L.T., Dung, N.T. and Duong, V.: Investigation of the mechanical dynamics of the PRV-1 machine gun installed on a combat robot, Advances in Military Technology, Vol. 21, No. 1, pp. 95-112, 2026.

[11] Truong, T.H., Macko, M., Nguyen, D.P. and Vu, D.T.: Effect of some structural parameters on the firing stability of the PKMS machine gun when firing with complicated boundary conditions, Proceedings of the 2021 International Conference on Military Technologies (ICMT 2021), IEEE, pp. 1–6, 2021.

[12] Van Dung, N., Van Bien, V., Van Thach, D. and Van Minh, P.: Dynamic modeling and stability analysis of bipod-mounted gas-operated machine guns, Noise & Vibration Worldwide, 2025, https://doi.org/10.1177/09574565251394418.

[13] Nguyen, D.P. and Macko, M.: Research technical solution for reducing oscillations of weapons mounted on the vehicle, Proceedings of the 2021 International Conference on Military Technologies (ICMT 2021), University of Defence, Brno, Czech Republic, IEEE, pp. 1–6, June 2021.

[14] Nguyen, P.D., Vo, B.V., Nguyen, P.M. and Tran, T.H.: Dynamics of automatic firing system type gas-operated weapon, Problemy Mechatroniki: Uzbrojenie, Lotnictwo, Inżynieria Bezpieczeństwa (Problems of Mechatronics: Armament, Aviation, Safety Engineering), Vol. 14, No. 4, pp. 9–22, 2023.

[15] Dang, B.N., Macko, M., Bui, V.D. and Bien, V.V.: Influence of certain structural parameters on the firing stability of the robot-weapon system on elastic ground, Advances in Military Technology, Vol. 21, No. 1, pp. 195-212, 2026.

[16] Doan, D.V., Bien, V.V, Quang, M.A. and Phu, N.M.: A study on multi-body modeling and vibration analysis for twin-barrel gun while firing on elastic ground, Applied Engineering Letters, Vol. 8, No. 1, 2023, https://doi.org/10.18485/aeletters.2023.8.1.5.

[17] Sy, N.T., Beer, S., Van Bien, V., Phon, N.D. and Phu, N.M.: Oscillation of the anti-tank missile system Fagot fired on the elastic ground, Proceedings of the 2019 International Conference on Military Technologies (ICMT 2019), University of Defence, Brno, Czech Republic, IEEE, pp. 1–5, May 2019.

[18] Balla, J., Dao, M.H., Truong, T.H., Nguyen, V.D. and Tran, V.T.: Firing stability of automatic grenade launcher mounted on tripod, Proceedings of the 2021 International Conference on Military Technologies (ICMT 2021), University of Defence, Brno, Czech Republic, IEEE, pp. 1–8, June 2021.

[19] Quang, M.A.: Investigation of the Effects of Selected Twin-Barrel Parameters on the Motion of the 37 mm K65 Twin-Barrel Anti-Aircraft Gun During Firing, PhD Thesis, Le Quy Don University of Technology, Hanoi, Vietnam, 2021.

[20] Wong, J.Y.: *Theory of ground vehicles*, 5th ed., John Wiley & Sons, Hoboken, New Jersey, USA, 2022.

[21] Borkowski, W., Figurski, J., Walentynowicz, J. and Hryciów, Z.: The impact of the cannon on the combat vehicle chassis during firing, Journal of KONES, Vol. 14, pp. 49–61, 2007.

[22] Balla, J., Havlicek, M., Jedlicka, L., Krist, Z. and Racek, F.: Firing stability of mounted small arms, International Journal of Mathematical Models and Methods in Applied Sciences, Vol. 5, No. 3, pp. 412–422, 2011.

[23] Balla, J.: Contribution to determining of load generated by shooting from automatic weapons, Proceedings of the 2019 International Conference on Military Technologies (ICMT 2019), University of Defence, Brno, Czech Republic, IEEE, pp. 1–6, May 2019.

[24] Bien, V.V., Phuc, T.V. and Macko, M.: Effect of some structural parameters on firing stability of shooter-weapon system, Advances in Military Technology, Vol. 16, No. 2, pp. 235-251, 2021.

[25] Tien, V.D., Macko, M., Procházka, S. and Bien, V.V.: Mathematical model of a gas-operated machine gun, Advances in Military Technology, Vol. 17, No. 1, pp. 63-77, 2022.

[26] Nguyen, D.V., Bui, V.Q., Nguyen, D.T., Uong, Q.S. and Truong, H.T.: Studying the thermo-gas-dynamic process in a muzzle brake compensator, Archive of Mechanical Engineering, Vol. 70, No. 2, pp. 311–328, 2023, https://doi.org/10.24425/ ame. 2023.145384.

[27] Éles, P.: Az 5,56 mm-es CZ BREN 2 gépkarabély, Haditechnika, Vol. 56, No. 2, pp. 7–12, 2022, https://doi.org/10.23713/HT.56.2.02.

NOMENCLATURE

DOF	Degrees of freedom
UGVs	Unmanned ground vehicles
PS0	Input parameters

Greek symbols

α	Azimuth angle
φ	Elevation angle
φ_1	Front shock absorber inclination angle relative to the vertical
φ_2	Rear shock absorber inclination angle relative to the vertical
η	Efficiency

ИСТРАЖИВАЊЕ СТАБИЛНОСТИ ПАЉБЕ БОРБЕНОГ РОБОТА НА ЕЛАСТИЧНОЈ ПОДЛОЗИ

Д.Б. Нгок, М. Мацко, Ј. Бала

Овај рад истражује вибрације система борбеног робота и оружја опремљеног аутоматским оружјем малог калибра током паљбе, на основу физичког и математичког модела развијеног коришћењем теорије динамике вишетелесних система. Просторни модел борбеног робота има шест степени слободе (DOF), обухватајући контролисаног робота опрем–љеног аутоматском пушком калибра 5,56 мм. Динамика оружја, представљена померањем основне везе, анализира се истовремено са вибрацијама целог система. Применом нумеричких метода за ре–шавање система диференцијалних једначина које описују вибрације изазване силама паљбе, узимајући у обзир еластична својства носећег тла, испитан је динамички одзив система робота и оружја. Експериментална мерења вибрација робота у равни паљбе показала су одлично слагање са теоријским симулацијама, потврђујући валидност предложеног модела. Предложени модел омогућава идентификацију кључних параметара који утичу на стабилност робота при паљби. Израчунати резул–тати показују разуман степен поузданости, пружа–јући научну основу за даља истраживања стабил–ности система и тачности оружја када се интегрише у борбеног робота.